

# Gutenberg-Richter-like relations in physical systems

K. Duplat,<sup>1</sup> G. Varas,<sup>2</sup> and O. Ramos<sup>1,\*</sup>

<sup>1</sup>*Institut Lumière Matière, UMR5306 Université Lyon 1-CNRS, Université de Lyon 69622 Villeurbanne, France.*

<sup>2</sup>*Instituto de Física, Pontificia Universidad Católica de Valparaíso (PUCV), Avenida Universidad 330, Valparaíso, Chile.*

(Dated: December 22, 2025)

We analyze regional earthquake energy statistics from the Southern California and Japan seismic catalogs and find scale-invariant energy distributions characterized by an exponent  $\tau \simeq 1.67$ . To quantify how closely scale-invariant dynamics with different exponent values resemble real earthquakes, we generate synthetic energy distributions over a wide range of  $\tau$  under conditions of constant activity. Earthquake-like behavior, in a broad sense, is obtained for  $1.5 \leq \tau < 2.0$ . When energy variations are further restricted to be within a factor of ten relative to real earthquakes, the admissible range narrows to  $1.58 \leq \tau \leq 1.76$ . We identify the physical mechanisms governing the dynamics in the different regimes: fault dynamics characterized by a balance between slow energy accumulation and release through scale-free events in the earthquake-like regime; externally supplied energy relative to a slowly driven fault for  $\tau < 1.5$ ; and dominance of small events in the energy budget for  $\tau > 2$ .

## I. INTRODUCTION

In many dissipative phenomena, including earthquakes [1], granular faults [2–7], sandpiles [8–10] and subcritical rupture [11–16], energy is slowly accumulated and then released through sudden events of all sizes, typically following power-law distributions. The scale-invariant nature of these events motivated theoreticians to draw on the formalism of phase transitions [17, 18]. Yet this raises a fundamental question: in natural systems, how is the fine-tuning of the order parameter required to reach criticality achieved? [17] The idea of a critical point acting as an attractor of the dynamics, introduced by the Self-Organized Criticality (SOC) in 1987 [18], offered a compelling and elegant answer.

Although SOC’s ambitious claims [19] and the absence of a unified theoretical framework attracted criticism [20, 21], the conceptual power of the idea galvanized leading figures in statistical physics [22, 23] and propelled its application to fields as diverse as seismology [24], neuroscience [25], and even financial markets [26].

Earthquakes were the most familiar, well-studied, and arguably the most relevant of these phenomena, and thus they quickly became the reference point for interpreting scale-invariant behavior. Regardless of the value of the power-law exponent  $\tau$  in the event-size distribution  $P(s) \sim s^{-\tau}$ , the underlying interpretation remained the same: events occur across all scales, with numerous small ones and rare, catastrophic ones that dominate the total energy release.

In the 1990s, most laboratory experiments and earthquake catalogs lacked the precision needed to confront or guide theoretical developments. Reported  $b$ -values in the Gutenberg-Richter (GR) law spanned a wide range [27], and no clear consensus existed on how to define an avalanche in a way that allowed meaningful comparison between theoretical or simulated  $\tau$  exponents and those extracted from real data.

From a theoretical standpoint, much of the effort focused on determining the value of  $\tau$  and classifying avalanches into

universality classes [28–32]. However, the extent to which the underlying dynamics differ across these classes was rarely examined, and they were often implicitly assumed to reflect the same earthquake-like behavior described above.

With the ultimate goal of understanding the precise physical scenario associated with a given exponent value, we begin by examining how avalanche sizes must be defined in order to compare them consistently. We then turn to the statistics of actual earthquakes, and finally analyze the different scenarios that arise when the exponent  $\tau$  of the earthquake-size distribution is varied.

## II. AVALANCHE DEFINITION

A central goal of this article is to clarify the physical scenarios associated with particular exponent values. As expected, however, different definitions of avalanche size lead to distinct event distributions [33]. Consider a power law of the form  $P(s) = \frac{1}{N} s^{-\tau_1}$ , where  $N$  is a normalization constant. The variable  $s$  can be expressed as  $s = s_l^{D_A}$ , where  $s_l$  is the linear extent of the avalanche and  $D_A$  its fractal dimension. Using this relation we obtain:

$$P(s)ds = P(s_l)ds_l \quad (1)$$

$$\frac{1}{N} s_l^{-\tau_1} D_A d_A s_l^{D_A-1} ds_l = P(s_l)ds_l \quad (2)$$

$$P(s_l) = \frac{D_A}{N} s_l^{-\tau_2}, \text{ where } \tau_2 = (\tau_1 - 1)D_A + 1. \quad (3)$$

Thus, the same underlying process can be described by two power laws,  $P(s)$  and  $P(s_l)$ , characterized by different exponents,  $\tau_1$  and  $\tau_2$ . Which definition should be considered the “correct” one? In the context of critical phenomena, event size is conventionally defined in terms of the event’s volume in an  $n$ -dimensional space [32, 34, 35]. Therefore, to meaningfully compare scale-invariant avalanche statistics with those of critical phenomena, *the avalanche size must be proportional to its volume*.

\* osvanny.ramos@univ-lyon1.fr

**Earthquakes as avalanches:** The *Seismic moment*  $M_0 = \mu Sd$  provides a direct measure of the potential energy released during an earthquake. Here,  $\mu$  denotes the shear modulus of the rocks,  $S$  is the rupture area along the fault, and  $d$  is the average slip [36]. The scale-invariant character of earthquakes stems from the broad range of scales observed in  $S$ . Consequently, when treating earthquakes as scale-invariant phenomena,  $M_0$  –which is proportional to the released energy– constitutes the appropriate definition of avalanche size.

### III. EARTHQUAKES STATISTICS

Catalogs report earthquake magnitudes  $M$ , typically derived directly from seismic moments, as a measure of event strength. From these magnitudes, the released energy  $E$  can be estimated using [37]:

$$\log(E) = 3/2(M + 6.07). \quad (4)$$

We analyze two local catalogs (Fig. 1):

- JMA catalog from the Japan Meteorological Agency [38]; Time interval: [1983-2023]; Region: Longitude 123°E – 163°E, Latitude 26°N – 50°N.
- SCECD catalog from the Southern California Earthquake Data Center [39]; Time interval: [1980-2025]; Region: Longitude 113.1°W – 121.7°W, Latitude 30.1°N – 39.3°N.

Most recent geophysical studies analyze the GR law locally, in both space and time (see an exhaustive analysis here [40]). Local variations may arise from statistical artifacts or from genuine changes in the physical conditions of the fault. Discrepancies among different earthquake catalogs are also a recognized issue, reflecting the difficulties in accurately measuring earthquake magnitudes [40]. To minimize these issues, we focus on the primary archives for the two selected regions and perform a global analysis. The data analysis begins with a completeness test, in which the minimum magnitude considered reliable for fitting is defined as the lowest value showing a stable detection rate over the selected time interval, corresponding to Magnitude  $M2 \equiv [M2.0, M2.9]$  in California and  $M5 \equiv [M5.0, M5.9]$  in Japan.

The GR law is defined as:

$$\log(N_c(M)) = a - bM, \quad (5)$$

where  $a$  and  $b$  are constants and  $N_c(M)$  is the (cumulative) number of earthquakes of magnitude  $M$  or greater. The GR relations for both regions, with  $N_c(M)$  expressed on a yearly basis, yield  $b$  values very close to 1.0 (Fig. 2a).

In most areas of physics, cumulative distributions are not the primary object of analysis, since they tend to obscure the physical mechanisms associated with events of a given size. Instead, differential (or noncumulative) distributions are usually preferred because they provide direct access to the statistics of events within a specific size range, allowing one to relate scaling exponents and distribution shapes more transparently to the underlying physical processes. In (Fig. 2b) we

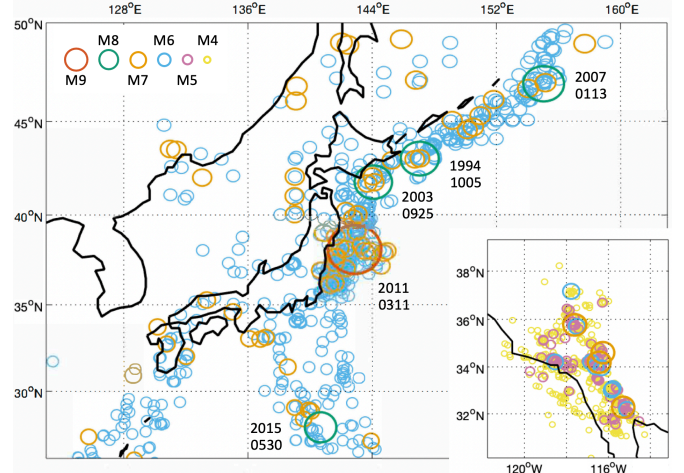


**Figure 1. Catalogs.** Regions analyzed in the JMA (Japan) and SCECD (Southern California) catalogs in the time-intervals reported in the text. All M6-M9 earthquakes in Japan and all M4-M7 earthquakes in Southern California are shown, with colors and symbol sizes indicating magnitude (see legend). The dates of the Tōhoku earthquake (M9.1) and the four M8 events in Japan are also indicated. The M8 earthquakes in Japan are used as reference events throughout the article.

define  $N(M)$  as the number of earthquakes of magnitude  $M$  per year, using integer intervals of magnitude values. The relation is similar to the GR relation,

$$\log(N(M)) = a_1 - b_1 M, \quad (6)$$

with, as expected, the  $b_1$  values being larger than their corresponding  $b$  values. The differences are negligible in this case; however, we will show in the next section that for smaller  $b$  values these differences become significant.

The scale-invariance of earthquakes is reflected in their energy distributions. Earthquake energy release is calculated from magnitude values using Eq. 4. Energy distributions follow power laws in the form  $P(E) \sim E^{-\beta}$ , with exponent values around  $\beta = 1.67$ , specifically  $\beta = 1.67$  for Japan and  $\beta = 1.68$  for Californian earthquakes (Fig. 2c). The time series of the cumulative energy release (Fig. 2d) further demonstrates that the largest earthquakes strongly dominate the total energy budget.

Figures 2e and f show extrapolations of the distributions of magnitudes and energies for Japan earthquakes. We have chosen for the analysis micro-earthquakes of M0.0 as a baseline (choosing a smaller minimum delivers similar results) and 8.9 as the maximum one. We have excluded the M9.1 Tōhoku earthquake (2011), because they have an average period of about a century, much larger than the time-interval of the analysis. We have used  $b_1 = 1$  and  $\beta = 1.67$  for the extrapolation. Notice that from Eqs. 4 and 6, we obtain  $\beta = 2b_1/3 + 1$ . In the context of scale-invariant avalanches the size exponent is denoted  $\tau$ . Thus  $\beta = \tau = 1.67$  is the size exponent for earthquake dynamics.

The extrapolation provides the  $K$  value of the distribution  $P(E) = KE^{-\tau}$ . As  $P(E) = N(E)\Delta E$ , where  $N(E)$  is the

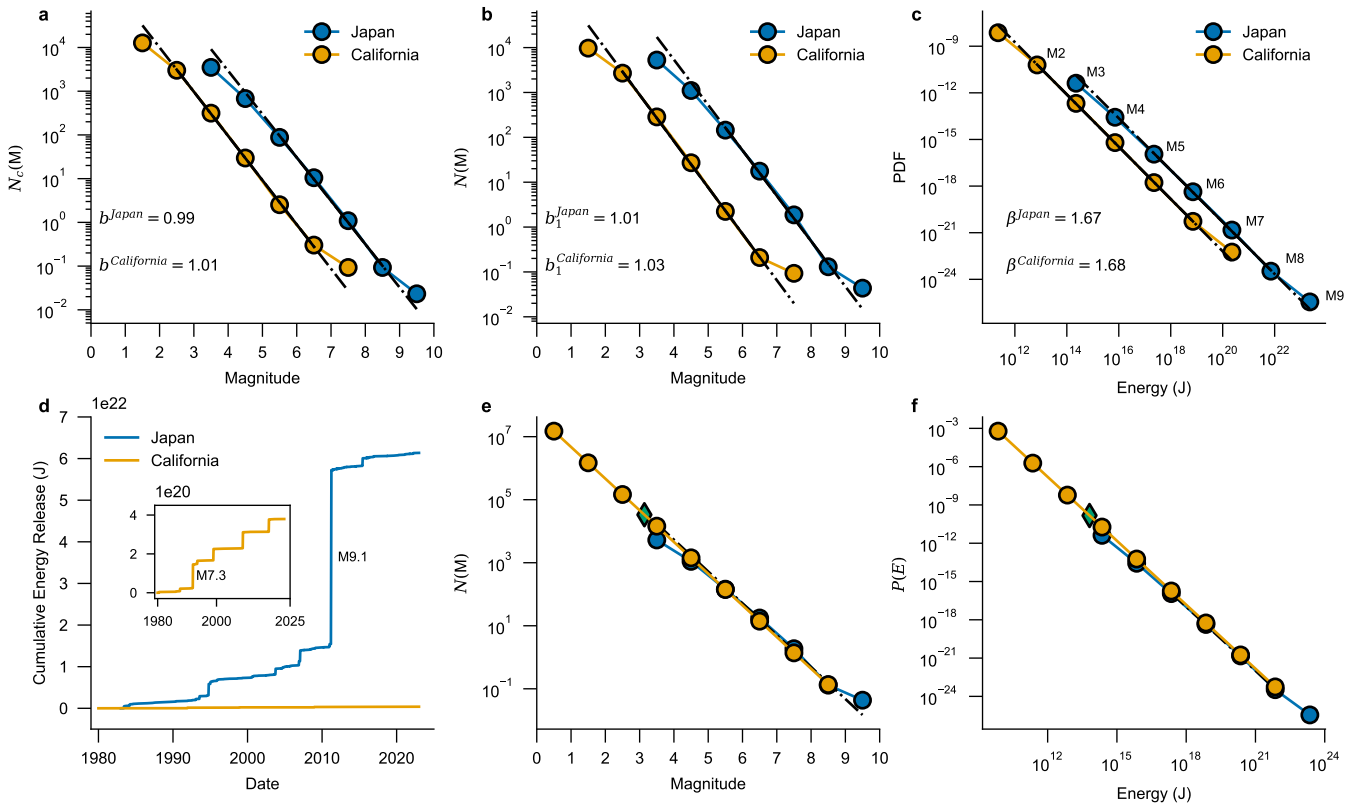


**Figure 2. Earthquakes statistics.** (a) Gutenberg-Richter relations (Eq. 5) for Japan (JMA catalog) and Southern California (SCEDC catalog). The fits correspond to the solid lines. Magnitudes smaller than  $M2 \equiv [M2.0, M2.9]$  in the SCEDC, and than  $M5$  in JMA, are affected by catalog incompleteness. (b) Non-cumulative number of earthquakes per year as a function of the magnitude (Eq. 6). (c) Non-cumulative energy distribution. They follow power law distributions with  $\beta$  values around 1.67. (d) Cumulative energy release. Notice that the Tōhoku earthquake (2011,  $M9.1$ ) accounts for more than 63 % of the total energy release in the period. Californian earthquakes release two orders of magnitude less energy. Four  $M7+$  quakes dominate the total energy release: Landers (1992,  $M7.3$ ), Hector Mine (1999,  $M7.1$ ), Baja California (2010,  $M7.2$ ), and Ridgecrest (2019,  $M7.1$ ). (e,f) Extrapolation of the relations obtained in panels (b) and (c) for Japan, assuming  $b_1 = 1$  and  $\beta = 1.67$  respectively.

annual number of earthquakes with a given energy, and  $\Delta E$  the width of the logarithm binning, we can use

$$N_{tot} = \sum P(E) \Delta E = \int P(E) dE \quad (7)$$

$$E_{tot} = \sum N(E) E = \int P(E) E dE \quad (8)$$

to calculate the total annual energy release of  $E_{tot} = 1.621 \times 10^{21}$  J and the total number of events of  $N_{tot} = 24\,819\,295$  events/year, corresponding to an average activity rate of  $N_{tot}^{-1} = 1.27$  s between events.

Considering a steady state, the input energy  $E_{in} = \langle E \rangle = E_{tot}/N_{tot}$ , which accounts for the energy stored in the fault in a time interval of 1.27 s. This corresponds to a mean magnitude value  $\langle M \rangle = M3.2$ , which is relatively small. The period of  $M8 \equiv [M8.0, M8.9]$  events is  $T_{M8} = 6.6$  years and they account for 67% of the total energy release  $E_{tot}$ .

Based on this information on real earthquakes in Japan, we can broadly define **earthquake-like behavior as a regime**

characterized by a relatively small input energy rate  $E_{in}$  leading to scale-invariant energy-release events, in which rare, extremely large events dominate the total energy budget  $E_{tot}$ .

#### IV. CHANGING EXPONENT VALUES

By keeping the limits  $M0.0$  and  $M8.9$  and considering a **constant activity** ( $N_{tot} = \text{const.}$ ), we have calculated the energy distributions for different exponent values (Fig. 3a). At first glance we can think that all of them represent earthquake-like dynamics. However, if we use Eq. 4 and translate the energy values into magnitudes (Fig. 3b) it is much easier to interpret the data.

To assess the validity of our definition and its degree of similarity to real earthquakes across different exponent values, we focus on three criteria: (i) how small the input energy rate  $E_{in}$  is (Fig. 3c); (ii) which events, and to what extent, control the total energy budget  $E_{tot}$  (Fig. 3d); and (iii) how rare catastrophic  $M8$  events are (Fig. 3e).

The dynamics for different values of  $\tau$  span regimes rang-

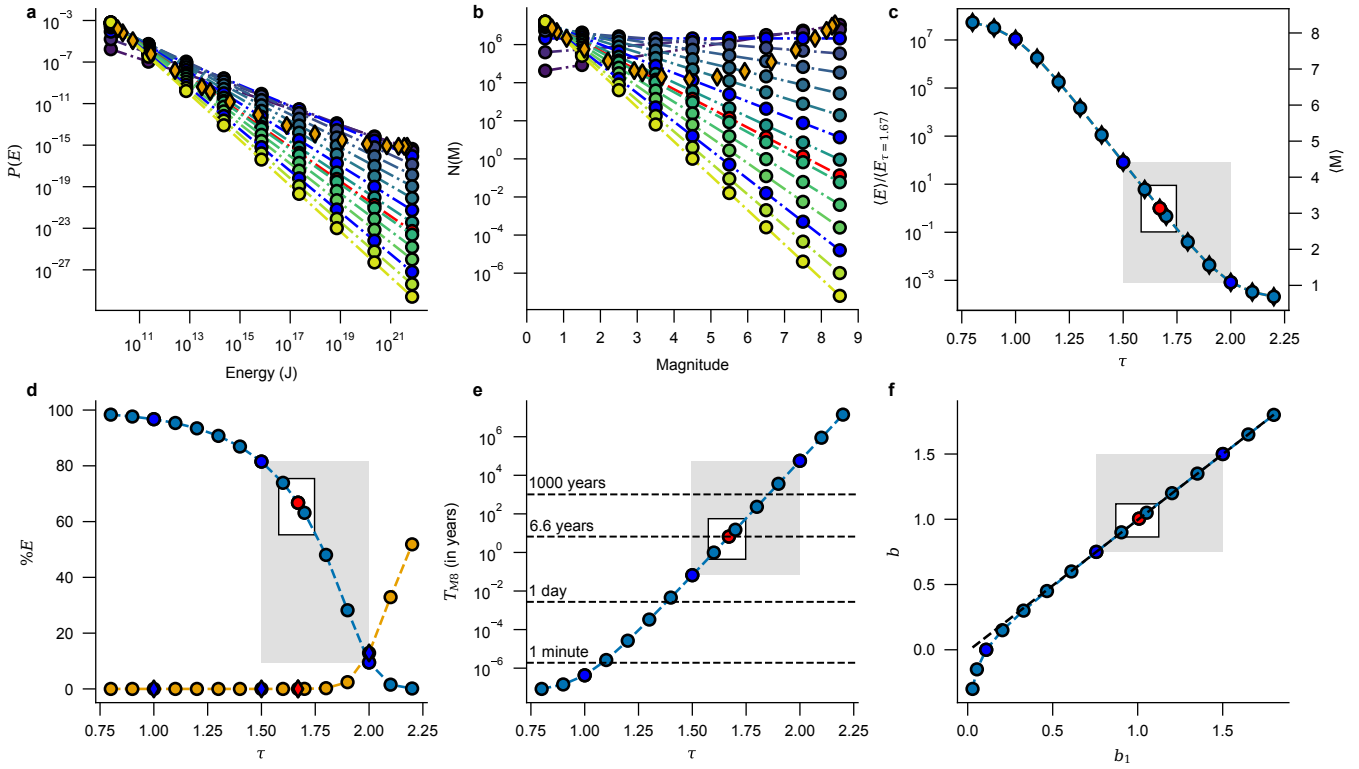


**Figure 3. Earthquake-like dynamics.** (a) Energy distributions for different exponent  $\tau$  values ranging from 0.8 to 2.2 (dark to bright colors) considering a constant activity and magnitudes  $M \in [M0.0 - M8.9]$ . In the case of  $\tau = 1.67$  (in red) it describes the energy distribution of Japan earthquakes. Curves with exponents  $\tau = 1.0, 1.5$  and  $2.0$  have been highlighted in blue. Orange diamonds correspond to the mean value of the released energy  $\langle E \rangle$ . (b) The same data in (a) expressed as number of earthquakes / year as a function of the magnitude. (c) Average energy release  $\langle E \rangle$  normalized by the average energy release for  $\tau = 1.67$ , and corresponding magnitude  $\langle M \rangle$  values as a function of the exponent. A gray rectangle indicates the *earthquake-like* regime, while the white rectangle indicates the range where the differences in  $\langle E \rangle$  are less than ten-times the one of real earthquakes. (d) Energy contributions (in %) of extreme magnitude events M8 (in blue) and M0 (in orange) as a function of the exponent value. At  $\tau = 1.67$ , 67% of the energy is released by the M8 events. However, for  $\tau > 2$  the energy budget is controlled by the smallest M0 events. (e) Average period of M8 earthquakes as function of  $\tau$ . (f)  $b$  value as function of  $b_1$ . The black dashed line has a slope equal 1.  $b$  starts to deviate from the identity at  $b_1 < 0.5$ , corresponding to  $\tau < 1.33$ .

ing from extremely high mean energies  $\langle E \rangle$ , of the order of the energy of the largest events (below  $\tau = 1.0$ ), to extremely low ones, above  $\tau = 2.0$  (Figs. 3a,b,c). At  $\tau = 1.5$ , where the  $\langle M \rangle = (M8.9 - M0.0)/2 \simeq M4.5$ , the values of  $\langle E \rangle$  split into two groups, corresponding to large and small energies (Fig. 3c). Consequently, we find **small** injected energies  $E_{in}$  for  $\tau \geq 1.5$ .

However, it is important to notice that the energy differences increase rapidly as  $\tau$  moves away from  $\tau = 1.67$ . If we restrict these differences to be within *ten-times* of the energy of real earthquakes, the exponent values corresponding to dynamics close to those of real earthquakes are limited to the range  $1.58 \leq \tau \leq 1.76$  (white rectangles in Fig. 3).

Figure 3d shows the percentage of energy released by the two extreme event classes, namely high-magnitude M8 and low-magnitude M0 events. The contribution of M8 events decreases rapidly for  $\tau > 1.8$ . At  $\tau = 2.0$ , all magnitudes contribute equally to the total released energy  $E_{tot}$ , while for  $\tau > 2.0$  the smallest events dominate the energy budget. Using the *ten-times* limits defined in the previous analysis, the percentages of energy released by M8 earthquakes are found

to be 75% and 54% (Fig. 3d), which are 12% larger and 13% smaller, respectively, than the energy release of real M8 earthquakes (67%).

The combined analysis of Figs. 3c and 3d indicates that our broad definition of earthquake-like behavior is valid only in the regime  $1.5 \leq \tau < 2.0$ , indicated by gray rectangles in Fig. 3.

The average period of M8 earthquakes under different exponent values (Fig. 3e) gives a clear indication of how different the scenarios become when we move away from  $\tau = 1.67$  where  $T_{M8} = 6.6$  years. Let us analyze the following **scenarios**:

$\tau = 1.0$ : In this case all magnitudes are equiprobable with events of each of them happening in average every 13 seconds. In order to supply the energy for generating M8 earthquakes every 13 s in average in Japan,  $\langle E \rangle$  is  $1.1 \times 10^6$  times larger than in the real earthquakes case, and corresponds to a M7.8 event. The scenario is quite far from the real earthquakes one. The energy cannot be slowly stored in the fault and predominantly liberated by rare extreme events. In this case the energy has to be always available to deliver an im-

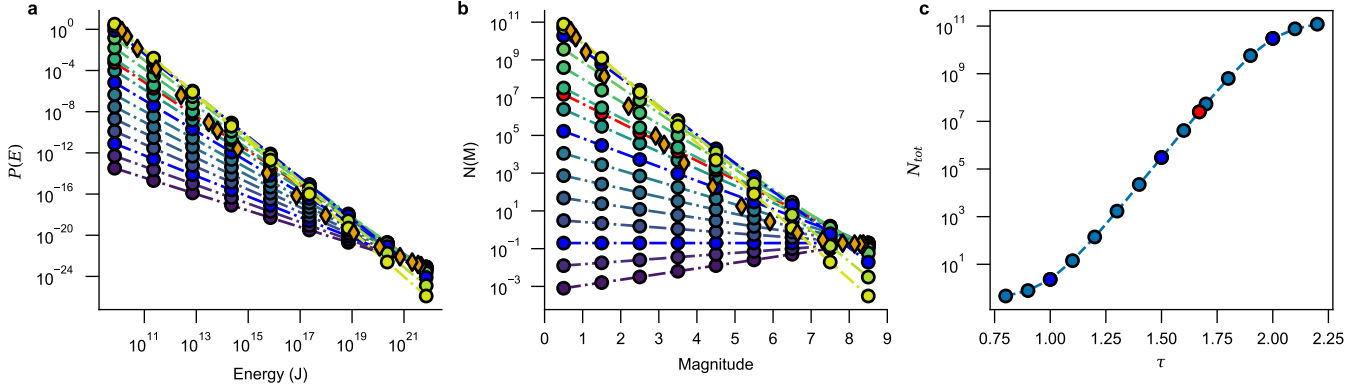


**Figure 4. Dynamics under constant energy.** (a) Energy distributions for different exponent  $\tau$  values ranging from 0.8 to 2.2 (dark to bright colors) considering a constant energy release and magnitudes  $M \in [M0.0 - M8.9]$ . In the case of  $\tau = 1.67$  (in red) it describes the energy distribution of Japan earthquakes. Curves with exponents  $\tau = 1.0, 1.5$  and  $2.0$  have been highlighted in blue. Orange diamonds correspond to the mean value of the released energy  $\langle E \rangle$ . (b) The same data in (a) expressed as number of earthquakes / year as a function of the magnitude. (c) Total number of events / year as a function of  $\tau$ .

minent extreme event, a behavior that can be found in some fracture experiments[15].

$\tau = 1.5$ : With this exponent value, M8 earthquakes will take place every 24 days in average in Japan.  $\langle E \rangle$  is 82 times larger than in the real earthquakes case, and corresponds to a M4.5.

$\tau = 1.9$ : In this case, M8 earthquakes will take place every 3611 years in average in Japan.  $\langle E \rangle$  is 232 times smaller than in the real earthquakes case, and corresponds to a M1.6 event. M8 events account for 28% of the energy release in the fault.

$\tau = 2.0$ : In this case, M8 earthquakes will take place every 56 490 years in average in Japan.  $\langle E \rangle$  is 1204 times smaller than in the real earthquakes case, and corresponds to a M1.1 event. All magnitudes contribute equally to the energy budget. For larger exponent values M0 magnitude events control the energy budget. This is an issue because in real systems, the smallest events are at the same level than the measurement noise, meaning that most of the energy is released at these small scales.

If we use the *ten-times* limits defined in the previous analysis, the  $T_{M8}$  limits correspond to 7 months and 81 years (Fig. 3f), which are 11,3 times smaller and 12,3 times larger with respect to the real earthquake value of  $T_{M8} = 6.6$  years in Japan.

Figure 3f shows the differences in  $b$  values in cumulative vs. non cumulative distributions. For large  $b$  values they are negligible, and only for  $b < 0.5$ , corresponding to  $\tau < 1.33$ , we see noticeable variations between the two distributions. In the earthquake-like regime of  $1.5 \leq \tau < 2.0$ , both distributions are very similar.

## V. DISCUSSION

All the previous analyses were carried out under the assumption of constant activity ( $N_{tot} = \text{const.}$ ). However, alternative scenarios can also be considered. Here, we focus on the opposite case, in which the total released energy is kept

constant ( $E_{tot} = \text{const.}$ ) and the annual number of events,  $N_{tot}$ , becomes the variable of interest.

The energy distributions obtained for different values of  $\tau$  (Fig. 4a) differ from those shown in Fig. 3a only by normalization factors. Under the condition  $E_{tot} = \text{const.}$ , the curves intersect at high energy values. Nevertheless, when considered individually, all distributions appear qualitatively similar. Independently of the normalization condition –whether constant activity or constant energy release– one might therefore be tempted to interpret all of them as earthquake-like dynamics, even for  $\tau < 1.0$ , a regime that has indeed been reported in fracture experiments [15].

Converting energies into magnitudes (Figs. 3b and 4b) allows for a more direct comparison with real earthquake statistics. In this representation, it becomes clear that for  $\tau < 1.0$

Table I. Dependence of energy release and M8 earthquake statistics on the exponent value  $\tau$ .

$\tau$	$\langle E \rangle / \langle E_{\tau=1.67} \rangle$	$E(M8) / E_{tot}$	$T_{M8}$
0.8	$5.4 \times 10^7$	98%	3 seconds
0.9	$3.2 \times 10^7$	97%	4 seconds
1.0	$1.1 \times 10^7$	96%	13 seconds
1.1	$1.8 \times 10^6$	95%	1.5 minutes
1.2	$1.8 \times 10^5$	93%	14 minutes
1.3	$1.4 \times 10^4$	91%	3 hours
1.4	$1.1 \times 10^3$	87%	40 hours
1.5	82	82%	24 days
<b>1.58</b>	<b>10</b>	<b>75%</b>	<b>7 months</b>
1.6	6	74%	1 year
<b>1.67</b>	<b>1</b>	<b>67%</b>	<b>6.6 years</b>
1.7	0.47	63%	15 years
<b>1.76</b>	<b>0.1</b>	<b>54%</b>	<b>81 years</b>
1.8	$4.0 \times 10^{-2}$	48%	232 years
1.9	$4.3 \times 10^{-3}$	28%	3611 years
2.0	$8.3 \times 10^{-4}$	10%	56490 years
2.1	$3.3 \times 10^{-4}$	2%	$8.9 \times 10^5$ years
2.2	$2.1 \times 10^{-4}$	0.1%	$1.4 \times 10^7$ years

small-magnitude events are less frequent than catastrophic ones, a behavior that is in strong contrast with observed earthquake catalogs.

For  $\tau = 1.0$ , where all magnitudes are equiprobable, the activity is extremely low, with  $N_{tot} \sim 2$  events per year (Fig. 4c). In this regime, the system spends most of its time accumulating energy, and events occur only rarely. This situation does not correspond to the scale-invariant dynamics commonly observed in experiments, which could otherwise be misinterpreted as earthquake-like behavior. More generally, for  $\tau < 1.5$ , the dynamics is characterized by reduced activity and long periods of energy accumulation without avalanches. In both experimental systems and real seismic data exhibiting scale invariance, the number of events is typically very large. For this reason, we consider the condition of constant activity ( $N_{tot} = \text{const.}$ ) to be more appropriate for describing and comparing different scale-invariant scenarios as the exponent  $\tau$  deviates from 1.67. Table I summarizes the energy-related quantities and the statistics of catastrophic M8 events. In doing so, it provides a quantitative measure of how close a given scale-invariant dynamics is to a real earthquake scenario.

In conclusion, we have analyzed earthquake statistics, with particular emphasis on energy distributions, and found an exponent value  $\tau \simeq 1.67$  in both the Southern California and Japan catalogs. This analysis leads to a relatively broad definition of earthquake-like behavior. Synthetic distributions generated for different  $\tau$  values under the condition of constant

activity indicate that this broad definition is valid only in the range  $1.5 \leq \tau < 2.0$ . When energy variations are further restricted to within *ten-times*, defining a practical closeness to real earthquake dynamics, the admissible range narrows to  $1.58 \leq \tau \leq 1.76$ .

Beyond providing a quantitative measure of proximity to real earthquake behavior, our results also reveal the distinct physical mechanisms associated with different exponent values. For  $1.5 \leq \tau < 2.0$ , the dynamics corresponds to the expected fault behavior, in which energy is slowly stored and released through events spanning all scales [6]. As  $\tau$  decreases, the increased frequency of large-energy events requires a substantial amount of available energy, which cannot be supplied by slow accumulation alone but, in the case of fracture experiments, may be stored in the elastic bulk of the system [15]. For  $\tau > 2.0$  [7], small events dominate the energy budget. In most real datasets, such events lie close to the noise level of measurements, making it difficult to reliably estimate the true energy release of the system.

## VI. ACKNOWLEDGMENTS

This work was supported by the ANR grant ANR-22-CE30-0046 and the CONYCIT cooperation project MEC80180053.

---

- [1] B. Gutenberg and C. F. Richter, Magnitude and energy of earthquakes, *Annali di Geofisica* **9**, 1 (1956).
- [2] K. E. Daniels and N. W. Hayman, Force chains in seismogenic faults visualized with photoelastic granular shear experiments, *J. Geophys. Res. Solid Earth* **113**, 2156 (2008).
- [3] T. A. Brzinski and K. E. Daniels, Sounds of failure: Passive acoustic measurements of excited vibrational modes, *Phys. Rev. Lett.* **120**, 218003 (2018).
- [4] A. Abed Zadeh, J. Barés, and R. P. Behringer, Crackling to periodic dynamics in granular media, *Phys. Rev. E* **99**, 040901 (2019).
- [5] A. Abed Zadeh, J. Barés, J. E. S. Socolar, and R. P. Behringer, Seismicity in sheared granular matter, *Phys. Rev. E* **99**, 052902 (2019).
- [6] S. Lherminier, R. Planet, V. Levy dit Vehel, G. Simon, L. Vanel, K. J. Måløy, and O. Ramos, Continuously sheared granular matter reproduces in detail seismicity laws, *Phys. Rev. Lett.* **122**, 218501 (2019).
- [7] D. Houdoux, A. Amon, D. Marsan, J. Weiss, and J. Crassous, Micro-slips in an experimental granular shear band replicate the spatiotemporal characteristics of natural earthquakes, *Communications Earth & Environment* **2**, 90 (2021).
- [8] V. Frette, K. Christensen, A. Malthe-Sørensen, J. Feders, T. Jøssang, and P. Meakin, Avalanche dynamics in a pile of rice, *Nature* **379**, 49 (1996).
- [9] E. Altshuler, O. Ramos, C. Martínez, L. E. Flores, and C. Noda, Avalanches in One-Dimensional Piles with Different Types of Bases, *Phys. Rev. Lett.* **86**, 5490 (2001).
- [10] O. Ramos, E. Altshuler, and K. J. Måløy, Avalanche prediction in a self-organized pile of beads, *Phys. Rev. Lett.* **102**, 078701 (2004).
- [11] K. J. Måløy, S. Santucci, J. Schmittbuhl, and R. Toussaint, Local waiting time fluctuations along a randomly pinned crack front, *Phys. Rev. Lett.* **96**, 045501 (2006).
- [12] J. Baró, Á. Corral, X. Illa, A. Planes, E. K. Salje, W. Schranz, D. E. Soto-Parra, and E. Vives, Statistical similarity between the compression of a porous material and earthquakes, *Phys. Rev. Lett.* **110**, 088702 (2013).
- [13] M. Stojanova, S. Santucci, L. Vanel, and O. Ramos, High frequency monitoring reveals aftershocks in subcritical crack growth, *Phys. Rev. Lett.* **112**, 115502 (2014).
- [14] I. G. Main, F. Kun, and A. F. Bell, Crackling noise in digital and real rocks—implications for forecasting catastrophic failure in porous granular media, in *Avalanches in Functional Materials and Geophysics*, edited by E. K. Salje, A. Saxena, and A. Planes (Springer International Publishing, 2017).
- [15] J. Barés, A. Dubois, L. Hattali, D. Dalmas, and D. Bonamy, Aftershock sequences and seismic-like organization of acoustic events produced by a single propagating crack, *Nature Communications* **9**, 1253 (2018).
- [16] Y. Xu, A. G. Borrego, A. Planes, X. Ding, and E. Vives, Criticality in failure under compression: Acoustic emission study of coal and charcoal with different microstructures, *Phys. Rev. E* **99**, 033001 (2019).
- [17] H. E. Stanley, *Introduction to Phase Transitions and Critical Phenomena* (Oxford Univ. Press, New York, 1987).
- [18] P. Bak, C. Tang, and K. Wiesenfeld, Self-organized criticality: An explanation of the  $1/f$  noise, *Phys. Rev. Lett.* **59**, 381 (1987).

[19] P. Bak, *How Nature works-The Science of Self-organized Criticality* (Oxford Univ. Press, Oxford, 1996).

[20] R. Frigg, Self-organised criticality-what it is and what it isn't, *Studies in History and Philosophy of Science Part A* **34**, 613 (2003).

[21] N. W. Watkins, G. Pruessner, S. C. Chapman, N. B. Crosby, and H. J. Jensen, 25 years of self-organized criticality: Concepts and controversies, *Space Science Reviews* **198**, 3 (2016).

[22] L. P. Kadanoff, A. B. Chhabra, A. J. Kolan, M. J. Feigenbaum, and I. Procaccia, Critical indices for singular diffusion, *Phys. Rev. A* **45**, 6095 (1992).

[23] P. W. Anderson, From the top down, *Nature* **383**, 772 (1996).

[24] I. Main, Statistical physics, seismogenesis, and seismic hazard, *Reviews of Geophysics* **34**, 433 (1996).

[25] J. M. Beggs and D. Plenz, Neuronal avalanches in neocortical circuits, *Journal of Neuroscience* **23**, 11167 (2003).

[26] J.-P. Bouchaud, The self-organized criticality paradigm in economics & finance (2024), arXiv:2407.10284 [q-fin.GN].

[27] P. Bak and C. Tang, Earthquakes as a self-organized critical phenomenon, *Journal of Geophysical Research: Solid Earth* **94**, 15635 (1989).

[28] Y.-C. Zhang, Scaling theory of self-organized criticality, *Phys. Rev. Lett.* **63**, 470 (1989).

[29] A. Vespignani, S. Zapperi, and L. Pietronero, Renormalization approach to the self-organized critical behavior of sandpile models, *Phys. Rev. E* **51**, 1711 (1995).

[30] S. Lübeck and K. D. Usadel, Numerical determination of the avalanche exponents of the bak-tang-wiesenfeld model, *Phys. Rev. E* **55**, 4095 (1997).

[31] A. Chessa, H. E. Stanley, A. Vespignani, and S. Zapperi, Universality in sandpiles, *Phys. Rev. E* **59**, R12 (1999).

[32] P. Le Doussal and K. J. Wiese, Size distributions of shocks and static avalanches from the functional renormalization group, *Phys. Rev. E* **79**, 051106 (2009).

[33] K. Duplat, A. Douin, and O. Ramos, Memory effects govern scale-free dynamics beyond universality classes, submitted.

[34] D. Stauffer and A. Aharony, *Introduction To Percolation Theory* (CRC Press, 2003).

[35] Z. Olami, H. J. S. Feder, and K. Christensen, Self-organized criticality in a continuous, nonconservative cellular automaton modeling earthquakes, *Phys. Rev. Lett.* **68**, 1244 (1992).

[36] H. Kanamori, The energy release in great earthquakes, *Journal of Geophysical Research (1896-1977)* **82**, 2981 (1977).

[37] T. C. Hanks and H. Kanamori, A moment magnitude scale, *J. Geophys. Res. B: Solid Earth* **84**, 2348 (1979).

[38] JMA Catalogue: [https://www.data.jma.go.jp/eqev/data/bulletin/hypo\\_e.html](https://www.data.jma.go.jp/eqev/data/bulletin/hypo_e.html).

[39] SCEDC Catalogue: [https://service.scedc.caltech.edu/eq-catalogs/date\\_mag\\_loc.php](https://service.scedc.caltech.edu/eq-catalogs/date_mag_loc.php).

[40] Y. Kamer and S. Hiemer, Data-driven spatial b value estimation with applications to california seismicity: To b or not to b, *J. Geophys. Res. Solid Earth* **120**, 5191 (2015).